

# Fully Integrated Fault-tolerance for PMSMs in Aviation Applications

Alastair P. Thurlbeck, Student Member, IEEE  
School of Electrical Engineering and Computer Science  
Oregon State University  
Corvallis, Oregon 97331  
Email: thurlbea@oregonstate.edu

Yue Cao, Member, IEEE  
School of Electrical Engineering and Computer Science  
Oregon State University  
Corvallis, Oregon 97331  
Email: yue.cao@oregonstate.edu

**Abstract**—An open-circuit fault-tolerant system implementation is presented for sensorless three-phase PMSM drives. The fault-tolerant system uses a fourth inverter leg connected to the motor neutral point, allowing for post-fault two-phase operation. Since the control is sensorless and fault detection is performed by the controller, no additional sensors are required beyond three phase current sensors. Hence, the fault-tolerant system is particularly suitable for highly integrated or compact drive systems. Whilst fault detection and sensorless two-phase control are well documented in existing literature, often little attention is given to the transitional behavior between a fault occurring and post-fault operation. Hence we focus on experimentally testing the fault-tolerant system in its entirety. An open-circuit fault is created during sensorless three-phase operation, causing a transient in the motor torque and speed. The controller rapidly detects the fault, and switches to post-fault control with the faulty leg disabled and the 4th leg connected to the motor neutral. In the test system the fault caused only a 5% dip in motor speed before the speed was smoothly regulated back to the commanded pre-fault speed under the post-fault two-phase control scheme. This fast recovery from a fault condition is particularly beneficial to aviation applications, where even a brief loss of the motor drive may be unacceptable.

**Index Terms**—Fault-tolerance, PMSM, Inverter, AC Motor Drives, Aviation

## I. INTRODUCTION

Permanent magnet synchronous machines (PMSMs) are widely used in aviation applications thanks to their high torque density and efficiency [1], [2]. PMSMs or brushless DC motors are also suitable as the electric propulsion motors in the emerging vertical-takeoff-and-landing urban aerial mobility vehicles. Each motor is typically driven by an “electronic speed controller” (ESC), which is an integrated voltage source inverter (VSI) and microcontroller drive system. When coupled with a lightweight propeller, such as those used in distributed propulsion, a high-efficiency high-power density motor drive is possible. In a distributed electric propulsion architecture, the propulsion motors and their drives are decentralized, enabling novel high efficiency fixed-wing aircraft designs such as NASA’s X-57 experimental all-electric aircraft. The X-57 spreads small high-lift motors along its wingspan along with larger cruise motors at its wingtips [3].

The closed-loop control of a PMSM or brushless DC motor relies on knowledge of the rotor angle and speed. For six-step

commutation, a hall effect sensor may be used, whilst field-orientated control typically requires an encoder. Alternatively, a sensorless control scheme may be applied, in which an estimator is used to provide an estimate of the rotor angle and speed from the measured phase currents and known motor parameters. The sensorless control scheme is advantageous, since the size and cost of the drive is reduced. Additionally, reliability is improved since position sensors add vulnerability to the drive system.

Complete fault detection, reconfiguration and post-fault control for an encoder equipped industrial PMSM was experimentally tested in [4]. However, the control was not sensorless and was implemented on a PC coupled dSpace controller board. Sensorless control and the transition from pre to post fault was demonstrated in [5]; however, fault-detection was omitted. In [6], a fault-tolerant fourth-leg inverter for aircraft electro-hydraulic actuators (EHAs) is presented. The authors give careful consideration to the transient behavior between a fault occurring and the steady state post-fault two-phase operation. However, the entire drive is briefly disabled to allow for fault-isolation and inverter reconfiguration. An encoder allows the two-phase drive to resume during the transient caused by the drive interruption, and such behavior may not be possible under a sensorless control scheme.

Hence we present an open-circuit fault-tolerant drive system for sensorless PMSM motor drives. In contrast to existing literature, experimental testing is performed on a minimalist controller and inverter setup, representative of the highly integrated drive systems common on most aerial vehicles. The only hardware modification required is the addition of a fourth inverter leg, which allows independent control of the remaining two healthy motor phases during post-fault [5], [7]–[10]. Following successful fault detection, the faulty inverter leg is isolated, and the fourth inverter leg is activated. Attention will be given to the transitional behavior from an open-circuit fault occurring, to the adoption of post-fault control, since this is the most challenging period for a sensorless control scheme.

The rest of the paper is organized as follows. Section II introduces the open-circuit detection scheme, and considers isolation requirements. Section III addresses the post-fault control strategy. Section IV discusses the fault-tolerant system implementation, considering the necessary hardware and con-

troller level modifications to realize the fault-tolerant system design. Section V validates the presented fault-tolerant system through extensive experimental testing.

## II. OPEN-CIRCUIT DETECTION AND ISOLATION

### A. Detection

Detection methods utilizing only the existing phase current measurements are advantageous, since no additional hardware sensors are required. Many open-circuit detection methods are based on monitoring the current space-vector trajectory in the alpha-beta frame [11]–[16]. During healthy three-phase operation, the current space vector follows a circular trajectory. However, when an open-circuit fault occurs the space vector becomes a semicircle, and thus various techniques may be applied to detect this condition, and localize the fault to one of the three phases. Such methods generally require averaging over one electrical period of the motor drive.

We adopt a recent alternative method proposed in [17] and demonstrated in [4], which instead considers the error between each of the phase current references and the actual phase currents measured by the controller. Whilst it still requires the same averaging time, it is unaffected by variations in the load. A diagnostic variable for each phase is found as:

$$d_{abc} = \frac{\langle i_{abc}^* - i_{abc} \rangle}{\langle |i_{abc}| \rangle} \quad (1)$$

During healthy operation all the diagnostic variables will be approximately zero. When an open-circuit fault occurs, the diagnostic variable of the affected phase converges to  $\pm 1$ , allowing for detection and localization. When a diagnostic variable crosses a fixed threshold, a fault is said to have occurred in the corresponding phase. A threshold of 0.85 is used in this paper. Whilst this detection scheme may also detect a short-circuit, it is too slow acting in doing so for practical usage.

The electrical period  $T_e$ , and therefore the approximate detection times, are calculated from the speed as follows:

$$T_e = \frac{2}{p} \cdot \frac{2\pi}{\omega_{mech}}, \quad (2)$$

where  $p$  is the number of motor poles and  $\omega_{mech}$  is the mechanical speed in rad/s.

### B. Isolation

During healthy three-phase operation, it is sufficient to simply disable the 4th inverter leg connected to the motor neutral. Whilst the body diodes of the 4th leg MOSFETs are still electrically connected, they are always reverse biased by the neutral point voltage. Following an open-circuit fault, the faulty phase leg should be disabled, and the 4th leg is now enabled to allow the use of the post-fault two-phase control scheme. However, the body diodes of the faulty phase leg now present an issue.

Since the 4th inverter leg uses PWM to control the neutral point voltage during post-fault control, the motor neutral point is now alternating between zero and the DC bus voltage at

the PWM switching frequency. Since the pole voltage of the faulty phase is the sum of the faulty phase back EMF and this alternating neutral point voltage, the body diodes of the faulty phase can be forward biased. During the positive half-cycle of the faulty phase back EMF, the upper MOSFET body diode conducts a current when the neutral point voltage is the DC bus voltage, and during the negative half-cycle, the lower MOSFET body diode conducts a current when the neutral point voltage is at zero. We emphasize that this current flow does not prevent the post-fault two-phase control scheme from operating effectively. However, performance will be slightly degraded since the post-fault currents are increased by the undesired current flow in the disabled faulty phase. To eradicate this issue, an isolation device such as a TRIAC or solid-state circuit breaker may be included in each phase line, and this device should be opened along with the faulty phase MOSFETs to fully isolate the faulty phase.

## III. POST-FAULT TWO-PHASE CONTROL THEORY

The post-fault control scheme allows optimal torque and speed control of the motor to be retained despite the disconnection of one of the motor phases. If the remaining two phase voltages are shifted to be  $60^\circ$  apart, and their magnitude is increased by a factor of  $\sqrt{3}$ , the rotating magnetic field created by the stator currents is unchanged from the 3-phase system [18]. This is facilitated by connecting the motor neutral to a 4th inverter leg controlled at the DC bus midpoint [9], [8]. Field-orientated control is used such that during post-fault, the controller behavior in the d-q frame is unchanged.

From healthy to post-fault operation, the inverse park transformation is modified to obtain modified post-fault voltage references  $V_{abc}^*$  [8], [19]. Equation (3) shows the post-fault transform for the 'a' phase fault case:

$$\begin{bmatrix} V_b \\ V_c \end{bmatrix} = \sqrt{3} \begin{bmatrix} \cos\left(\theta - \frac{2\pi}{3} - \frac{\pi}{6}\right) & -\sin\left(\theta - \frac{2\pi}{3} - \frac{\pi}{6}\right) \\ \cos\left(\theta + \frac{2\pi}{3} + \frac{\pi}{6}\right) & -\sin\left(\theta + \frac{2\pi}{3} + \frac{\pi}{6}\right) \end{bmatrix} \begin{bmatrix} V_d \\ V_q \end{bmatrix} \quad (3)$$

As in the healthy drive, the d-q axis currents control the rotor field and electromagnetic torque respectively. Torque ripple will be comparable to pre-fault levels, provided feedforward compensation is modified according to the faulted phase. The post-fault d-q machine equations are obtained for an 'a' phase fault as [8]:

$$\begin{aligned} V_{dq} = T_{bc2dq} \left[ R_s T_{bc2dq}^{-1} i_{dq} + w_e \frac{\partial L_{bc}}{\partial \theta} T_{bc2dq}^{-1} i_{dq} \right. \\ \left. + L_{bc} \frac{d}{dt} \left( T_{bc2dq}^{-1} i_{dq} \right) + w_e \psi_{bc} \right] \end{aligned} \quad (4)$$

Where:

$$\begin{aligned} V_{dq} &= \begin{bmatrix} V_d \\ V_q \end{bmatrix} & i_{dq} &= \begin{bmatrix} i_d \\ i_q \end{bmatrix} & \psi_{bc} &= \begin{bmatrix} -\lambda_{fd} \sin\left(\theta - \frac{2\pi}{3}\right) \\ -\lambda_{fd} \sin\left(\theta + \frac{2\pi}{3}\right) \end{bmatrix} \\ T_{bc2dq} &= \frac{2}{3} \begin{bmatrix} \cos\left(\theta - \frac{2\pi}{3}\right) & \cos\left(\theta + \frac{2\pi}{3}\right) \\ -\sin\left(\theta - \frac{2\pi}{3}\right) & -\sin\left(\theta + \frac{2\pi}{3}\right) \end{bmatrix} \\ L_{bc} &= \frac{1}{3} \begin{bmatrix} L' - \Delta L \cos\left(2\theta + \frac{2\pi}{3}\right) & -\frac{1}{2}L' - \Delta L \cos(2\theta) \\ -\frac{1}{2}L' - \Delta L \cos(2\theta) & L' - \Delta L \cos\left(2\theta - \frac{2\pi}{3}\right) \end{bmatrix} \end{aligned}$$

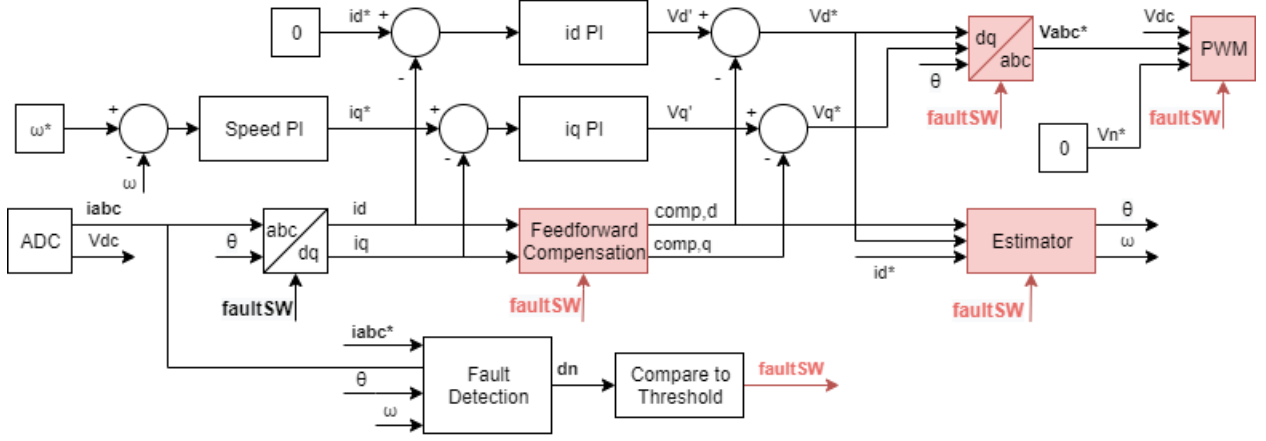


Fig. 1. Overview of the Fault-tolerant control scheme. Shaded blocks show where the equations are modified to switch from healthy three-phase control to post-fault two-phase control.

Where:

$$L' = L_d + L_q \quad \Delta L = L_q - L_d.$$

Assuming steady state operation such that  $\frac{di_d}{dt} = \frac{di_q}{dt} = 0$ , solving (4) gives post-fault feedforward compensation terms for the 'a' phase fault:

$$V_{comp,d} = \frac{\hat{w}_e}{3} \left( -2L_q i_q + L_q i_q \cdot \cos(2\theta) + (L_d i_d + \lambda_{fd}) \cdot \sin(2\theta) \right) \quad (5)$$

$$V_{comp,q} = \frac{\hat{w}_e}{3} \left( +2L_d i_d - L_q i_q \cdot \sin(2\theta) + (L_d i_d + \lambda_{fd}) \cdot \cos(2\theta) + 2\lambda_{fd} \right) \quad (6)$$

Sensorless control may be retained under post-fault operation by considering the altered post-fault machine model [5], [8]. To implement a phase locked loop type estimator post-fault, we substitute the estimated angle  $\hat{\theta}$  for  $\theta$  in the transformation  $T_{bc2dq}$ . Then (4) is solved, followed by substitution of (5) and small angle approximations. The angle error  $\tilde{\theta}$  is then given by [8]:

$$\tilde{\theta} \approx \frac{V_d^* - R_s i_d^* - V_{comp,d}}{\frac{2}{3} \hat{w}_e (\lambda_{fd} - \Delta L i_d^*)} \quad (7)$$

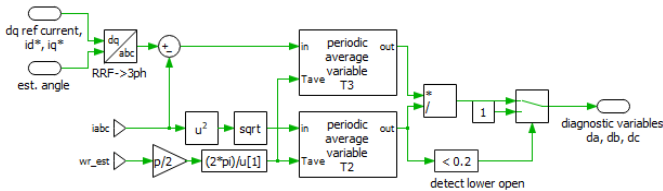


Fig. 2. Implementation of the open circuit detection scheme in PLECS. A periodic average is used where the averaging time is continually updated according to the estimated speed.

The negative angle error  $-\tilde{\theta}$ , calculated from (7) then drives a PI controller to generate the estimated angle  $\hat{\theta}$  and the estimated speed  $\hat{w}_e$ .

#### IV. FAULT-TOLERANT SYSTEM IMPLEMENTATION

##### A. Controller

The controller was implemented as a PLECS schematic, and was first validated through hardware in the loop simulation using the PLECS RTBox system. The PLECS coder allows the microcontroller to be programmed with code built directly from the controller schematic.

Fig. 1 shows a simplified representation of the fault-tolerant controller, where the shaded blocks are triggered by the "faultSW" signal to transition from healthy to post-fault control. Note that the presented equations for the post-fault two-phase control scheme are phase dependent. The equations shown above are correct only for an 'a' phase fault, and the additional equations for 'b' and 'c' phase faults must also be included in the controller. Similarly, whilst Fig. 1 shows a single 'faultSW' generated by the detection scheme, in practice there would be a 'faultSW' signal for each phase. When an open-circuit fault occurs, the correct post-fault control equations should be selected based on which 'faultSW' signal goes high.

Also not shown by the diagram is control for isolation and inverter reconfiguration. During healthy operation, the enable signals of the 'a', 'b' and 'c' phases will be high, whilst the enable signal for the 4th leg will be low. When the 'faultSW' signal changes the control equations, it also sets the enable signal for the faulty phase low. The 4th leg should be enabled in response to any 'faultSW' signal as part of the post-fault control adoption. If additional isolation devices are present in the inverter, they should also be controlled by the 'faultSW' or enable signals.

As Fig. 1 demonstrates, the fault-tolerant control scheme benefits from the field-oriented control, since the control in the d-q frame is largely unchanged from pre to post-fault

operation. Indeed, the PI controllers, which regulate the  $d$  and  $q$  axis currents and the  $d$  and  $q$  axis voltages, do not need to be altered. However, their gains can be modified for post-fault control if alterations to the post-fault closed-loop behavior are desired. The feedforward compensation is altered however, and its use is critical in stabilizing the post-fault control and preventing excessive torque ripple.

Fig. 2 shows the PLECS subsystem for the fault detection scheme, which corresponds to the "Fault Detection" block in Fig. 1. Note that since the control scheme operates in the  $d$ - $q$  frame, the reference phase currents must first be obtained as the inverse Park transformation of the  $d$ - $q$  current references. Since, averaging must occur over an electrical period, the current electrical period must first be calculated from the estimated speed. A periodic average is performed, in which the averaging time is continually updated. Hence the expected detection time is between one and two electrical periods.

### B. Motor and Inverter Modifications

To allow for post-fault operation, the motor must be wye terminated, with an accessible neutral point that can be connected to the fourth inverter leg. At a minimum, the inverter must be modified to have a fourth phase leg. Some three-phase inverters may only use two current sensors, since this is sufficient to obtain the three phase currents under balanced three-phase operation. However, post-fault control requires a current sensor for each phase, since under post-fault operation, the remaining two phases will require their own current sensor. As discussed earlier, additional isolation devices in each phase line are optional. Considering only open-circuit faults, their absence will slightly degrade the post-fault system performance. However, should the fault-tolerance be extended to short-circuit faults, isolation devices are necessary.

## V. EXPERIMENTAL TESTING

The hardware shown in Fig. 3 was used to experimentally test the complete fault-tolerant system. The controller was implemented on a TI LAUNCHXL-F28069M development board, whilst two TI BOOSTXL-DRV8323RH three-phase inverter boards were used to create a 4th leg inverter (two phase legs on the second board were unused). In a real system implementation, a custom inverter should be designed, however, the testing demonstrates that the only required modification is to add an extra phase leg. Whilst it was not included in this demonstration, a real implementation should consider adding isolation devices such as TRIACS or solid-state circuit breakers in each of the phase lines. Our testing demonstrates that whilst they are not necessary for the post-fault control to function, performance is slightly degraded due to an undesired post-fault current flow through the faulty phase's MOSFET body diodes.

The test motor is an Anaheim Automation BLY341S brushless DC motor. This motor was selected since it allows for a neutral point connection. Since the motor is brushless DC, its back EMF is more trapezoidal than the sinusoidal back EMF of a PMSM that the control scheme is designed for.

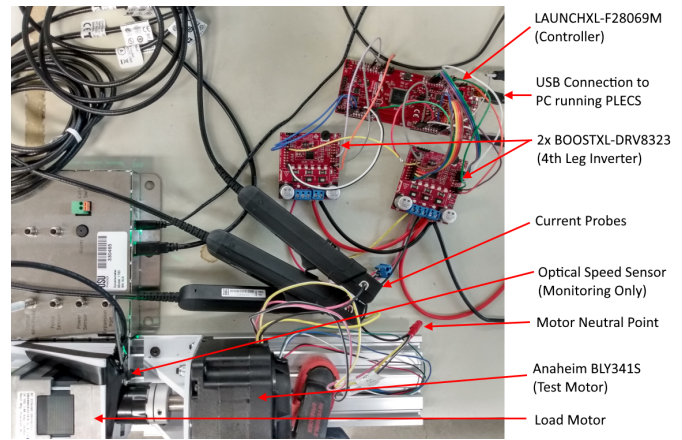


Fig. 3. Experimental test setup for demonstrating the complete fault-tolerant system. A 4th leg inverter is created by using three phase legs on one inverter board and a single phase leg on the other. The motor neutral point is connected to the 4th inverter leg to allow for post-fault two-phase control. The control is sensorless and does not require an encoder. The optical speed sensor is only used to provide external measurement of the true motor speed during the testing.

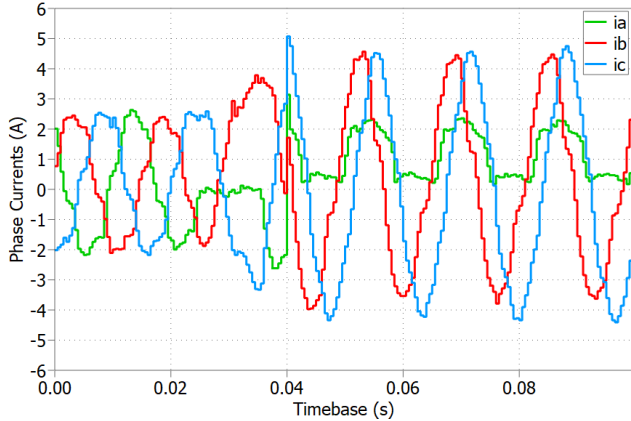
The test motor is connected to a second brushless DC motor, which acts as a simple load motor. The load motor is used to create a resistive load, which is driven by its back EMF. Hence the load motor provides a load torque that increases linearly with the test motor speed. Oscilloscope current probes are used to monitor the phase currents directly. An external optical speed sensor is used to observe the actual motor speed during hardware testing, but this speed measurement is not provided to the controller. We emphasize that the controller itself is sensorless, and instead uses an estimator to track angle and speed for the entirety of the hardware testing.

The controller was implemented in a PLECS schematic and was programmed directly to the MCU using the PLECS coder. Using PLECS external mode, the real-time controller signals during the hardware test may be directly observed via scopes in the PLECS interface. In this mode the scopes behave like an oscilloscope and may be triggered from a signal edge. PLECS external mode also allows for controller parameters to be changed in real-time from the PC, and this functionality is used to control the commanded speed and trigger the open-circuit fault. To trigger an open-circuit fault, the control signal for the 'a' phase upper MOSFET is disabled. Following this action, the controller must detect the fault using the open-circuit detection scheme, as if the fault had occurred naturally. Following successful fault detection, the controller should adopt the post-fault control scheme, disabling the 'a' phase leg and enabling the 4th inverter leg connected to the motor neutral point.

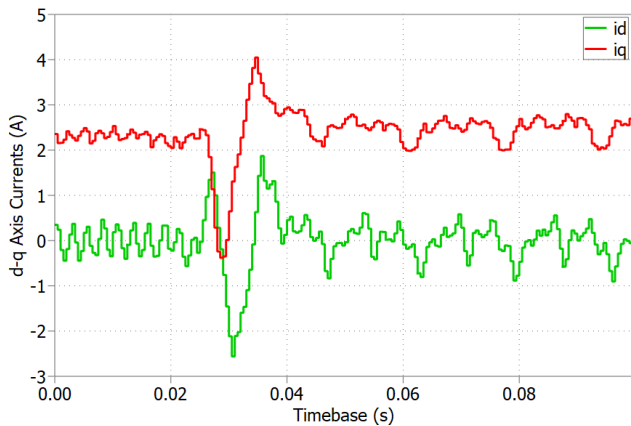
### A. Open-Circuit Detection and Transition to Post-fault Two-phase Control

In this test, the motor is initially operating under healthy three-phase control at a commanded speed of 100 rad/s. An open-circuit fault is created, and the controller must

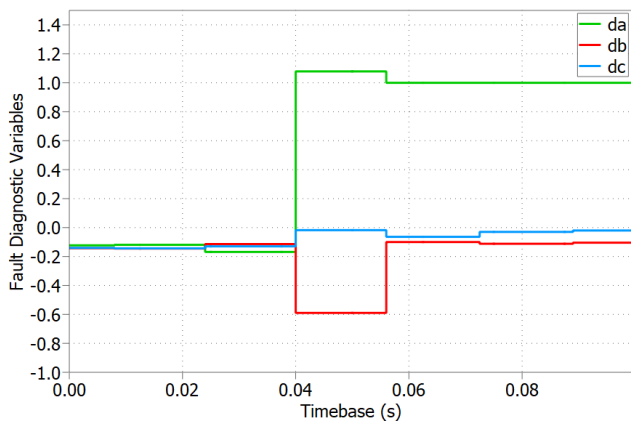
successfully detect the fault condition using the open-circuit detection scheme. Subsequently post-fault control is adopted with the faulty phase disabled and the 4th leg connected to the motor neutral enabled. This verifies not only the fault detection scheme, but also the behavior of the fault-tolerant



(a)

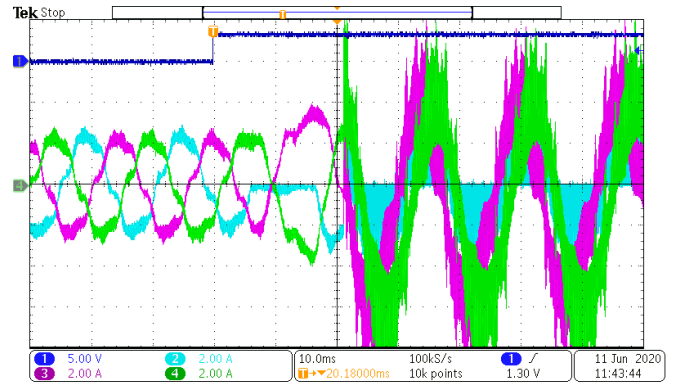


(b)

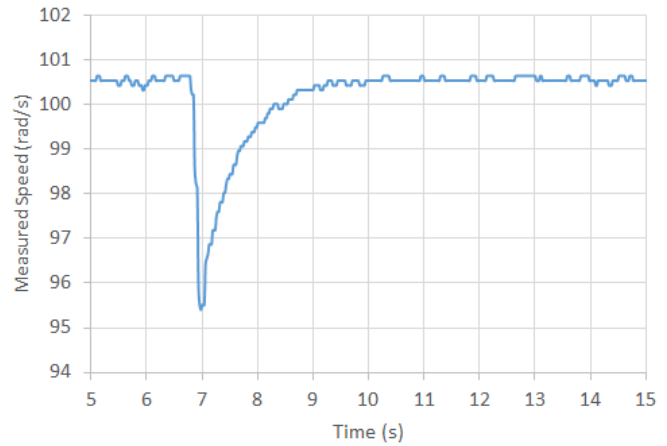


(c)

Fig. 4. Controller signals during the complete hardware test of the fault-tolerant system, in which the system must detect an open-circuit fault and transition to post-fault control with minimal loss of motor speed. (a) Sampled phase currents. (b) Transformed d-q axis currents. (c) Detection scheme diagnostic variables for each phase.



(a)



(b)

Fig. 5. Additional measurements during the complete hardware test of the fault-tolerant system, in which the system must detect an open-circuit fault and transition to post-fault control with minimal loss of motor speed. (a) Oscilloscope measurements: Blue = Trigger signal from the MCU to indicate that the fault has been created; Cyan =  $i_a$ ; Magenta =  $i_b$ ; Green =  $i_c$ . (b) Motor shaft speed measured by an external optical speed sensor.

drive in transitioning from healthy to post-fault control under the sensorless control scheme. If the detection and transition to post-fault control is successful, then the motor should return to the commanded 100 rad/s following the fault.

The open-circuit fault is triggered by disabling the 'a' phase upper MOSFET control signal within the microcontroller. Simultaneously, the controller sets an unused digital output high, which the oscilloscope may trigger from. This trigger signal is the voltage trace (Channel 1 in blue) in Fig. 5(a), and marks the moment at which the fault occurs. This corresponds to around 0.02s on the controller scope timebase in Fig. 4. In Fig. 5(a), the cyan trace (Channel 2) shows the measured 'a' phase current at zero due to the faulted 'a' phase upper MOSFET preventing the positive half-cycle. This is also observed by controller in the sampled phase currents of Fig. 4(a). The fault occurrence causes a transient event in the transformed d-q axis currents, shown in Fig. 4(b) around 0.03s.

Immediately following the fault occurrence, the fault has yet to be detected, and thus the controller is still trying to drive the motor using the healthy three-phase control scheme.

As the torque production of the motor is interrupted, a rapid loss of speed occurs, as shown by the external speed sensor measurement in Fig. 5(b). Fig. 4(c) shows the diagnostic variables of the controller open-circuit detection scheme. At 0.04s, the ‘a’ phase diagnostic variable converges to 1, crossing the fault detection threshold of 0.85. The controller thus adopts the post-fault two-phase control scheme corresponding to an ‘a’ phase fault at 0.04s. Hence the detection time was around 20 ms. At 100 rad/s, the electrical period and therefore averaging time of the detection scheme was 15.7 ms. At this moment the ‘b’ and ‘c’ phase currents can be observed to jump to a 60 degrees phase separation, and their magnitude is increased compared to the healthy three-phase control. The transformed d-q axis currents show this achieves relatively constant d-q axis currents as desired. Hence electromagnetic torque production is restored to the pre-fault level, albeit with slightly increased ripple. Fig. 5(b) shows the motor speed is restored to the commanded 100 rad/s, following the adoption of post-fault control at around  $t = 7$  s. Since isolation devices are not included in this demonstration, the ‘a’ phase body diodes are still electrically connected under post-fault control. The PWM modulated neutral voltage combined with the ‘a’ phase back EMF to cause an undesired current flow in the disabled phase. This is observable in the oscilloscope waveforms, and causes significant noise on the post-fault ‘b’ and ‘c’ phase currents.

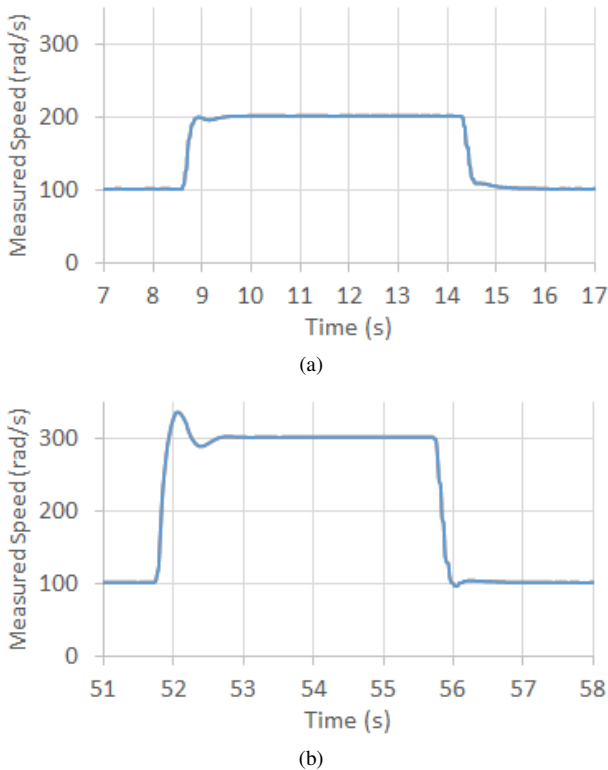


Fig. 6. Motor shaft speed measured by the external speed sensor under post-fault two-phase control. (a) Commanded speed steps from 100 to 200 rad/s and from 200 to 100 rad/s. (b) Commanded speed steps from 100 to 300 rad/s and from 300 to 100 rad/s.

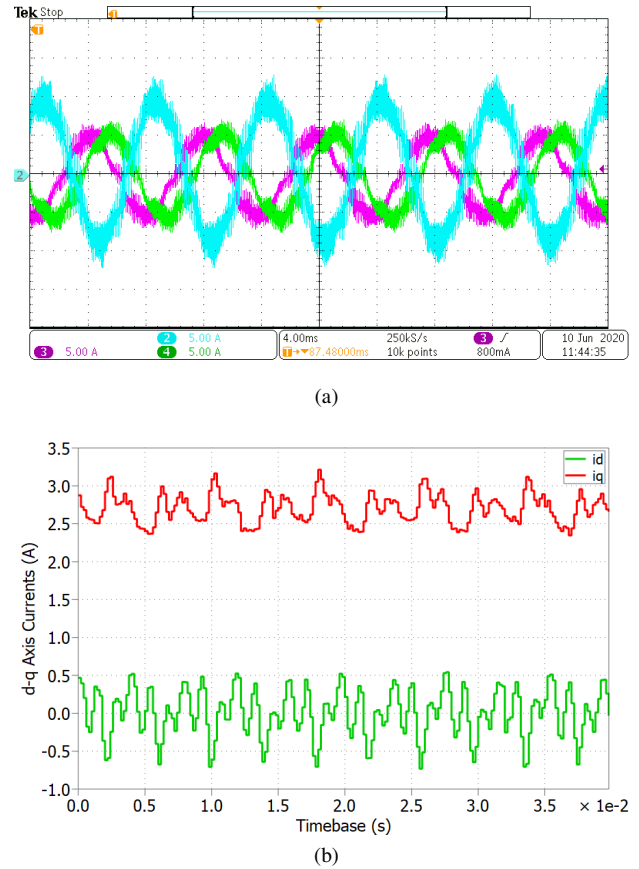


Fig. 7. Steady state operation under post-fault two-phase control at a commanded mechanical speed of 200 rad/s. (a) Oscilloscope measurements: Cyan =  $i_{neutral}$ ; Magenta =  $i_b$ ; Green =  $i_c$ . (b) Controller d-q axis currents.

### B. Behavior under Post-Fault Two-phase Control

Now that the successful detection and transitional behavior of the fault-tolerant system has been demonstrated, we also wish to demonstrate the efficacy of the post-fault two-phase control scheme. In these following tests, it is assumed that the faulted ‘a’ phase has completely electrically isolated from the rest of the drive. The addition of isolation devices such as TRIACs or solid-state circuit breakers would be required to achieve this. Otherwise the body diodes of the ‘a’ phase MOSFET would allow a current flow in the disabled phase, as was observed in the post-fault currents of the previous test (Fig. 4(a) and Fig. 5(a)).

Fig. 6(a) shows speed step responses from 100 to 200 rad/s and from 200 to 100 rad/s under the post-fault two-phase control scheme. Fig. 6(b) shows speed step responses from 100 to 300 rad/s and from 300 to 100 rad/s. Fig. 7 shows the steady-state behavior of the post-fault control scheme at 200 rad/s. Fig. 7(a) shows the oscilloscope measured ‘b’ phase (pink), ‘c’ phase (green) and 4th leg to neutral (cyan) currents. The controller sampled phase currents are transformed into the d and q axis currents shown in Fig. 7(b). The post-fault two-phase control demonstrates good closed-loop performance, with fast responses to the step inputs. Since the current magnitudes are significantly increased compared to pre-fault

operation, post-fault operation may be speed or torque limited compared to the pre-fault operation.

## VI. CONCLUSION

A complete open-circuit fault-tolerant system for sensorless three-phase PMSMs in aviation applications has been presented. The fault-tolerant system was experimentally tested in its entirety. The system was required to rapidly detect an open-circuit fault, and then successfully transition to post-fault operation with minimal loss of motor speed. When the open-circuit fault occurred at 100 rad/s, motor speed briefly decreased by 5 rad/s due to a loss of torque production. However, following the successful fault detection, post-fault control was adopted by disabling the faulty phase, and enabling the 4th inverter leg connected to the motor neutral. Under the post-fault control scheme the speed was smoothly regulated back to 100 rad/s. This transitional behavior is highly desirable, since it allows the motor to ride through the fault with only a brief interruption of motor torque production, which is crucial in an aviation application. Additional experimental tests further investigated the performance of the post-fault control scheme. Speed step responses demonstrated optimal closed-loop behavior under the post-fault control scheme.

The fault-tolerant system was implemented on existing controller and inverter hardware, demonstrating that this solution is appropriate for highly integrated PMSM drive systems in which no encoder is used, and additional sensors are undesirable. In practice, existing inverter designs may easily be modified to have an additional 4th inverter leg. It was found that whilst the post-fault performance would be improved by adding isolation devices to the inverter hardware, this was not a requirement for the post-fault control to function. Indeed, in many compact integrated drive systems, the inclusion of isolation devices would likely be space and cost prohibitive, and would decrease the efficiency of the drive. However, isolation devices are a necessity should short-circuit fault-tolerance be desired beyond the open-circuit fault-tolerance considered within this paper.

## REFERENCES

- [1] Z. Q. Zhu and D. Howe, "Electrical machines and drives for electric, hybrid, and fuel cell vehicles," *Proceedings of the IEEE*, vol. 95, no. 4, pp. 746–765, 2007.
- [2] *Introduction to Traction Machines*. John Wiley Sons, Ltd, 2017, ch. 6, pp. 159–177. [Online]. Available: <https://onlinelibrary.wiley.com/doi/abs/10.1002/9781119063681.ch6>
- [3] N. K. Borer, M. D. Patterson, J. K. Viken, M. D. Moore, J. Bevirt, A. M. Stoll, and A. R. Gibson, *Design and Performance of the NASA SCEPTOR Distributed Electric Propulsion Flight Demonstrator*. [Online]. Available: <https://arc.aiaa.org/doi/abs/10.2514/6.2016-3920>
- [4] J. O. Estima and A. J. M. Cardoso, "Fast fault detection, isolation and reconfiguration in fault-tolerant permanent magnet synchronous motor drives," in *Proc. IEEE Energy Conversion Congress and Exposition (ECCE)*, Sep. 2012, pp. 3617–3624.
- [5] A. Gaeta, G. Scelba, and A. Consoli, "Sensorless vector control of pm synchronous motors during single-phase open-circuit faulted conditions," *IEEE Transactions on Industry Applications*, vol. 48, no. 6, pp. 1968–1979, Nov 2012.
- [6] F. Richardeau, J. Mavier, H. Piquet, and G. Gateau, "Fault-tolerant inverter for on-board aircraft eha," in *Proc. European Conference on Power Electronics and Applications*, 2007, pp. 1–9.

- [7] B. Mirafzal, "Survey of fault-tolerance techniques for three-phase voltage source inverters," *IEEE Transactions on Industrial Electronics*, vol. 61, no. 10, pp. 5192–5202, 2014.
- [8] O. Wallmark, L. Harnefors, and O. Carlson, "Control algorithms for a fault-tolerant pmsm drive," *IEEE Transactions on Industrial Electronics*, vol. 54, no. 4, pp. 1973–1980, Aug 2007.
- [9] S. Bolognani, M. Zordan, and M. Zigliotto, "Experimental fault-tolerant control of a pmsm drive," *IEEE Transactions on Industrial Electronics*, vol. 47, no. 5, pp. 1134–1141, Oct 2000.
- [10] N. Bianchi, S. Bolognani, M. Zigliotto, and M. Zordan, "Innovative remedial strategies for inverter faults in ipm synchronous motor drives," *IEEE Transactions on Energy Conversion*, vol. 18, no. 2, pp. 306–314, 2003.
- [11] R. Peugeot, S. Courtine, and J. . Rognon, "Fault detection and isolation on a pwm inverter by knowledge-based model," *IEEE Transactions on Industry Applications*, vol. 34, no. 6, pp. 1318–1326, 1998.
- [12] A. M. S. Mendes and A. J. Marques Cardoso, "Voltage source inverter fault diagnosis in variable speed ac drives, by the average current park's vector approach," in *Proc. IEEE International Electric Machines and Drives Conference, IEMDC*, 1999, pp. 704–706.
- [13] F. W. Fuchs, "Some diagnosis methods for voltage source inverters in variable speed drives with induction machines - a survey," in *29th Annual Conference of the IEEE Industrial Electronics Society*, vol. 2, 2003, pp. 1378–1385.
- [14] K. Rothenhagen and F. W. Fuchs, "Performance of diagnosis methods for igbt open circuit faults in voltage source active rectifiers," in *IEEE 35th Annual Power Electronics Specialists Conference*, vol. 6, 2004, pp. 4348–4354.
- [15] K. Rothenhagen and F. W. Fuchs, "Performance of diagnosis methods for igbt open circuit faults in three phase voltage source inverters for ac variable speed drives," in *European Conference on Power Electronics and Applications*, 2005, pp. 10 pp.–P.7.
- [16] B. Lu and S. K. Sharma, "A literature review of igbt fault diagnostic and protection methods for power inverters," *IEEE Transactions on Industry Applications*, vol. 45, no. 5, pp. 1770–1777, 2009.
- [17] J. O. Estima and A. J. Marques Cardoso, "A new algorithm for real-time multiple open-circuit fault diagnosis in voltage-fed pwm motor drives by the reference current errors," *IEEE Transactions on Industrial Electronics*, vol. 60, no. 8, pp. 3496–3505, Aug 2013.
- [18] J. F. Eastham, "Igbt behavior during desat detection and short circuit fault protection," in *Proc. IEEE/MAS Annual Meeting 11*, 1998, pp. 748–751.
- [19] Tian-Hua Liu, Jen-Ren Fu, and T. A. Lipo, "A strategy for improving reliability of field-oriented controlled induction motor drives," *IEEE Transactions on Industry Applications*, vol. 29, no. 5, pp. 910–918, Sep. 1993.